Supporting Information

Capoen et al. 10.1073/pnas.1107912108

SI Materials and Methods

Plant Material and Fungal and Bacterial Strains. *Medicago truncatula* seedlings were transformed with *Agrobacterium rhizogenes* strain ARqua as previously described (1). Only one root expressing the cotransformation marker per plant was retained. After 1 wk in germination pouches (Anchor Paper), roots were inoculated with *Sinorhizobium meliloti* 1021 pXLGD4 (OD 0.05). Nodules were scored 21 d after inoculation. For mycorrhizal experiments, *Glomus intraradices* aseptic spores were produced as previously described (2). Transformed chimeric plants were transferred on 1:1 Terragreen (Oil-Dri UK) and low nutrient seed compost (Levington Horticulture), and 250 purified spores per root were applied. Six weeks after inoculation, root samples were taken and stained with ink (3). Colonization levels were measured using the gridline intersection method as previously described (4). Briefly, the roots are spread out over a Petri plate with a 1 × 1-cm grid pattern; where the root system intersects the gridline, presence or absence of intraradical colonization is scored. This allows for a straightforward assessment of total root colonization by determining the ratio between colonized and noncolonized root sections. One replicate was done using 5% Endorize Mix (granular mycorrhizal inoculum, Biorize R&D) mixed with TerraGreen and sand with identical results. For transient expression, *Nicotiana benthamiana* plants were grown, and leaves were infiltrated with *Agrobacterium tumefaciens* C58C1 pCH32 as previously described (5).

Sequence and Statistical Analysis. BLAST analysis using *Arabidopsis* calcium ATPase sequences (6) revealed several ATPase genes in the database. *MCA8* was found on a BAC sequence (GenBank accession no. AC186136), and the deduced ORF was submitted to GenBank (TPA BK007879). Error bars are as indicated. Briefly, bar graphs show the mean of the population tested, with the sample number shown as n. Error bars are SEM unless otherwise indicated. The scatterplot in Fig. 4 (main text) shows the individual roots as dots on the graph, with the mean + SEM shown as lines within the scatterplot; representative traces of this experiment are shown in Fig. 4*B* (main text). Where shown, paired t tests assuming unequal variance were done using GraphPad Prism 4.0 software.

Calcium Imaging. Analysis of calcium spiking was done as previously described (7). Micropipettes were pulled from filamented capillaries on a pipette puller (model 773, Camden Instruments). These were loaded with Oregon Green 488 BAPTA-1-dextran 10,000 kD or 70,000 kD and Texas Red-dextran 10,000 kD (Invitrogen), and cells were injected using iontophoresis with currents generated from a cell amplifier (model Intra 767, World Precision Instruments) equipped with a stimulus generator made to our specifications (World Precision Instruments). Cells were analyzed on an inverted epifluorescence microscope (TE2000, Nikon) using a monochromator (Optoscan, Cairn Research) to generate specific wavelengths of light. Images were captured with a CCD camera (ORCA-ER, Hamamatsu) and fluorescent data analyzed using Metaflor (Molecular Devices).

For analysis of calcium spiking using yellow cameleon, all roots were treated with Nod factor 30 min before imaging; this was to ensure that we could reliably measure calcium oscillations before excessive bleaching of the cameleon occurs, which could result in false negative results. From previous experience and previously published work we know that most cells (up to 90%) are responding to Nod factor with calcium oscillations within this time period. This permits us to say that most responsive cells will be showing robust calcium oscillations at this time, whereas cells lacking calcium oscillations are not due to a late onset of the calcium spiking response but rather due to the cell being unresponsive to Nod factor.

For the time-lapse confocal scanning images, the fluorescence was measured with a Zeiss LSM 510 Meta confocal scanning microscope equipped with a Plan-Aprochromat 0.80 oil-immersion objective 25× (Zeiss). The yellow cameleon calcium sensor was excited with the argon ion 458-nm laser and imaged using emission filters 476–486 nm for CFP and 529–540 nm for YFP. The time-lapse images were acquired at 73-ms intervals, the scanning resolution to 512 × 512 pixels, and the scan zoom to 10.6.

For experiments using a nuclear-targeted cameleon, the binary plasmid p35S:NupYC-Kan containing the nuclear-targeted yellow cameleon calcium sensor (8) (kindly provided by D. Barker, Institut National de la Recherche Agronomique–Centre National de la Recherche Scientifique Castanet, Tolosan Cedex, France) was used for *M. truncatula* hairy root transformation (1). For the time-lapse confocal scanning images, the fluorescence was measured with a Zeiss LSM 510 Meta confocal scanning microscope equipped with a Plan-Aprochromat 0.80 oil-immersion objective 25× (Zeiss). The transformed root hair cells of the nuclear-targeted yellow cameleon calcium sensor was excited with the argon ion 458-nm laser and imaged using emission filters 476–486 nm for CFP and 529–540 nm for YFP. The time-lapse images were acquired at 177-ms intervals, the scanning resolution to 512 × 512 pixels, and the scan zoom to 7.4.

Mathematical Modeling. The fire-diffuse-fire formulation of the reaction diffusion equation takes advantage of the fact that cluster sizes are extremely small compared with the size of the nucleus. For this reason, clusters can be considered to be point sources. This approximation means there is an exact expression for the concentration of calcium at any position on the surface of the nucleus at any time. This expression is a superposition of Green's functions. The solution of this form of the diffusion equation therefore does not require any type of finite difference scheme or any other similar numerical routine.

Because we seek solutions over the course of several seconds, and the typical times for which a channel cluster is open is on the order of milliseconds, we take the opening and closing of a cluster to be instantaneous. To accurately match experiments, we allow for temporal and spatial variation in cluster release quantities. We investigated parameter values for release quantities between 2 and 20 μmol and for the calcium uptake rate from 0.1 to 4 μM/s. We step forward in time on the order of tenths of milliseconds, and we say that a cluster will fire if the local Ca^{2+} concentration is above a given threshold. We take the threshold to be 50 nM above the ambient basal Ca^{2+} concentration, although for the stochastic simulations we allow this value to be a random variable. We explored values of this random variable between 0 and 5 μM. The refractory period during which a cluster must rest after firing is typically chosen to be approximately a quarter second, but again we allow this to take on random values between 0.1 s and 1 s for the stochastic simulation of spike initiation. The average distance between clusters is ≈5.5 μm (in agreement with data from oocytes; ref. 9) regardless of whether clusters are distributed randomly or evenly across the nuclear envelope. This means that for a nucleus of radius 12 μm, we place 60 clusters, and for a nucleus of radius 8 μm, we use 24 clusters. We remark that once the cluster locations have been

chosen, there is a relationship between the maximal minimum intercluster distance, the release quantities, the firing threshold, the diffusion rate, and the pump rate that will ensure a propagating wave. This relationship was used to guide parameter space exploration. To compute the flux through a pore we use Fick's law of diffusion, replacing the derivative with a finite difference between the concentrations on the inner and outer sides of the pore. This approach limits the transfer of calcium through the pore to diffusion alone, and so local pore conductance is determined by the local calcium difference and the pore diameter. We used a diffusion constant of 20 $\mu m^2/s$, and we took the cylindrical height of the pores to be 5 nm and the diameter to be 9 nm, the normal resting (nondilated) aperture (10), but allowed this value to vary up to close to the aperture of a fully dilated pore (0.026 nm). By varying these parameters, we investigated scenarios that include local calcium gradients at or above physiological levels, creating cases in which local pore conductance is highly heterogeneous.

For the graphical output, we create two ellipses whose semimajor axis is twice their semiminor axis. The ellipse is pixelated by first subdividing it latitudinally into 180 rows. We then place as many square pixels in each row as can fit so that the center of every pixel is within the ellipse. The center of each pixel is then coordinated with a point on the spherical nucleus. The exact solution is computed in FORTRAN for every pixel according to a user-defined timestep. Python code was written to produce the individual frames, and the movies were assembled using ffmpeg.

Antibody Production, Immunoblotting, and Immunohistochemistry. To raise a polyclonal antiserum against MCA8, a peptide (MGKGGENYGRKENTSC) was designed and used to immunize rabbits by Eurogentec and subsequently purified using the Sulfolink immobilization kit for peptides (Thermo Scientific), as described by the manufacturer.

Total proteins were prepared by homogenizing plant tissues on ice with extraction buffer [50 mM Hepes-KOH (pH 7.5), 100 mM sodium chloride, 10 mM EDTA, and 0.5 M sucrose] containing Complete protease inhibitor (Roche). The homogenate was centrifuged at 6,000 × *g* for 10 min. The extracted proteins were separated on 10–12% SDS/PAGE and transferred onto a PVDF membrane. For the immunoblots, an anti-rabbit horseradish peroxidase secondary antibody was used. Enhanced chemiluminescent reagent (GE Healthcare) was used to detect the proteins.

Immunohistochemical analysis was done as follows. Roots were fixed in 4% paraformaldehyde and embedded in paraffin after going through an ethanol and xylene dilution series. Sections (10 μm) were mounted on polylysine-coated microscope slides and deparaffinated and rehydrated before blocking for 3 h in 3% BSA in PBS. Slides were incubated with primary antibody in blocking buffer for 1 h with a 1:20 dilution. Slides were washed at least six times before incubating with goat anti-rabbit AlexaFluor 488 antibody (Invitrogen) for 1 h. Slides were then incubated with DAPI before being washed at least six times before mounting in Citifluor and imaging.

Immunohistochemistry on purified nuclei was done as above; nuclei were obtained as previously described (11).

Histology and Microscopy. β-Glucuronidase (GUS) assays were done and cleared with chloral hydrate as previously described (12). For inhibitors, concentrations used were chosen empirically; concentrations in a range similar to what is known from the literature were tested, and the lowest concentration with a clear effect was used in further experiments. At these concentrations plants looked healthy, and no effects on root hair morphology were visible. Plants were pretreated with inhibitors for 1 h before refreshing the medium with fresh inhibitor and 1 nM Nod factor. Roots were treated for 5 h before staining for GUS and clearing.

Sections (100 μm) for imaging were obtained by embedding nodules in 6% agarose before sectioning with a Vibratome and imaging on the Leica SP2 confocal microscope. Semithin 2-μm sections were made as previously described (12).

Transmission Electron Microscopy. The binary vector construct pRedRootII:DMI1:GFP was used to express the DMI1:GFP fusion protein under control of 35S constitutive promoter in *M. truncatula* Jemalong A17 plants (13). The fusion construct was delivered into the plant by *A. rhizogenes* MSU440 through "hairy root" transformation (1). *M. truncatula* roots (wild type and transgenic) were high-pressure frozen in a Baltec HPM 010 unit (Technotrade) and cryo-substituted in 0.2% uranyl acetate (Electron Microscopy Sciences) plus 0.2% glutaraldehyde (Electron Microscopy Sciences) in acetone at −80 °C for 72 h and warmed to −50 °C for 24 h. After several acetone rinses these samples were infiltrated with Lowicryl HM20 (Electron Microscopy Sciences) during 72 h and polymerized at −50 °C under UV light for 48 h. Sections were mounted on Formvar-coated nickel grids and blocked for 20 min with a 10% (wt/vol) solution of nonfat milk in Tris-buffered saline (TBS) containing 0.1% Tween-20. The sections were incubated in either anti-MCA8 antibodies or preimmune serum, or monoclonal anti-GFP antibody to localize DMI1 (1:10 in TBS–Tween-20 in all of the cases) for 1 h, rinsed in TBS containing 0.5% Tween-20, and then transferred to the secondary antibody (anti-mouse IgG 1:10 for anti-GFP; and anti-rabbit IgG 1:10 for anti-MCA8) conjugated to 15-nm gold particles for 1 h. To ascertain the relative preference for outer or inner nuclear membranes, a line was traced between these two nuclear membranes (equidistant to both membranes), and the distance between this line and the center of the gold particles was measured. The quantitative analysis of gold particle distribution in the nuclear membrane was done with the Image J program (http://rsbweb.nih.gov/ij/).

Phylogenetic Analysis. We used HMMbuild (14) to build a profile Hidden Markov Model with the 10 MCA proteins and used it with HMMsearch (13) to mine the *Lotus japonicus* (http://www.kazusa.or.jp/lotus/) and soybean (http://soybeangenome.org/) predicted protein sequences. The multiple sequence alignment was done using MUSCLE 3.7 (15) and edited with Jalview (16) and GeneDoc (17). The phylogenetics analysis was performed using the programs seqboot, protdist, neighbor, and consense in Phylip 3.69 (18). The tree was visualized in Mega4 (19).

Expression Analysis. Quantitative RT-PCR was done on a Bio-Rad Opticon DNA engine with the SYBR Green Jumpstart ready mix (Sigma) according to the manufacturer's instructions. One representative result is shown. As a reference gene, the EST sequence TC97716 was used because of its stable expression levels (20). Primers (Sigma) used were as follows: TC97716: AACGAATTTTCGCGTCAAAG and AGAACGGGACCAAGTTGTTG; MCA8: TTGGCTTGGTATGATGGTGA and AAAGCCTCCAAAGCCTTCTC; MtRR4: ATGCTTTTGTTCCGGGTTTA and CTGCACCTTCCTCCAAACAT.

Fusion Protein Localization. GFP fusion constructs were designed as follows. A truncated version of *MCA8* containing the predicted nuclear localization signal and three transmembrane regions was amplified using GCCAACTGGGGTCAATGC and ATCTGATTTTTGCTTTGATCTTCTTGC. Obtained vectors were sequence verified and recombined into pK7WGF2 for N-terminal GFP fusion (Invitrogen) (21) and transformed into *A. tumefaciens*.

RNAi-Mediated Knockdown of *MCA8*. For *MCA8*, a fragment of the 3′ UTR was amplified using GAAGAGGTGGCCTCAACACCA and GTTCGCACATACTTCCTGTGCATC. All fragments were designed with TOPO cloning-compatible primers

and cloned into the pENTR/D-TOPO vector (Invitrogen). Obtained vectors were sequence verified, and hairpin constructs were made by LR recombination with pK7WGIGW2-R (21) (containing DsRed as a transformation marker).

1. Boisson-Dernier A, et al. (2001) *Agrobacterium rhizogenes*-transformed roots of *Medicago truncatula* for the study of nitrogen-fixing and endomycorrhizal symbiotic associations. *Mol Plant Microbe Interact* 14:695–700.
2. St-Arnaud MC, Hamel C, Vimard B, Caron M, Fortin JA (1996) Enhanced hyphal growth and spore production of the arbuscular mycorrhizal fungus *Glomus intraradices* in an in vitro system in the absence of host roots. *Mycol Res* 100:328–332.
3. Vierheilig H, Coughlan AP, Wyss U, Piche Y (1998) Ink and vinegar, a simple staining technique for arbuscular-mycorrhizal fungi. *Appl Environ Microbiol* 64:5004–5007.
4. Giovannetti M, Mosse B (1980) An evaluatione of techniques for measuring VA mycorrhizal infections in roots. *New Phytol* 84:489–500.
5. Sparkes IA, Runions J, Kearns A, Hawes C (2006) Rapid, transient expression of fluorescent fusion proteins in tobacco plants and generation of stably transformed plants. *Nat Protoc* 1:2019–2025.
6. Baxter I, et al. (2003) Genomic comparison of P-type ATPase ion pumps in *Arabidopsis* and rice. *Plant Physiol* 132:618–628.
7. Wais RJ, et al. (2000) Genetic analysis of calcium spiking responses in nodulation mutants of *Medicago truncatula*. *Proc Natl Acad Sci USA* 97:13407–13412.
8. Sieberer BJ, et al. (2009) A nuclear-targeted cameleon demonstrates intranuclear Ca^{2+} spiking in *Medicago truncatula* root hairs in response to rhizobial nodulation factors. *Plant Physiol* 151:1197–1206.
9. Keener JP (2006) Stochastic calcium oscillations. *Mathematical Medicine and Biology* 23:1–25.
10. Alberts B, et al. (2008) *Molecular Biology of the Cell* (Garland Science, New York), 5th Ed.
11. McKeown P, Pendle AF, Shaw PJ (2008) Preparation of *Arabidopsis* nuclei and nucleoli. *The Nucleus: Nuclei and Subnuclear components*, ed Hancock R (Humana Press, New York).
12. Capoen W, et al. (2009) Calcium spiking patterns and the role of the calcium/calmodulin-dependent kinase CCaMK in lateral root base nodulation of *Sesbania rostrata*. *Plant Cell* 21:1526–1540.
13. Riely BK, Lougnon G, Ané JM, Cook DR (2007) The symbiotic ion channel homolog DMI1 is localized in the nuclear membrane of *Medicago truncatula* roots. *Plant J* 49: 208–216.
14. Eddy SR (1998) Profile hidden Markov models. *Bioinformatics* 14:755–763.
15. Edgar RC (2004) MUSCLE: Multiple sequence alignment with high accuracy and high throughput. *Nucleic Acids Res* 32:1792–1797.
16. Waterhouse AM, Procter JB, Martin DM, Clamp M, Barton GJ (2009) Jalview version 2—a multiple sequence alignment editor and analysis workbench. *Bioinformatics* 25:1189–1191.
17. Nicholas KB, Nicholas HBJ, Deerfield DWI (1997) GeneDoc: Analysis and visualization of genetic variation. *EMBNEW.NEWS* 4.
18. Retief JD (2000) Phylogenetic analysis using PHYLIP. *Methods Mol Biol* 132:243–258.
19. Tamura K, Dudley J, Nei M, Kumar S (2007) MEGA4: Molecular evolutionary genetics analysis (MEGA) software version 4.0. *Mol Biol Evol* 24:1596–1599.
20. Benedito VA, et al. (2008) A gene expression atlas of the model legume *Medicago truncatula*. *Plant J* 55:504–513.
21. Karimi M, Inzé D, Depicker A (2002) GATEWAY vectors for *Agrobacterium*-mediated plant transformation. *Trends Plant Sci* 7:193–195.

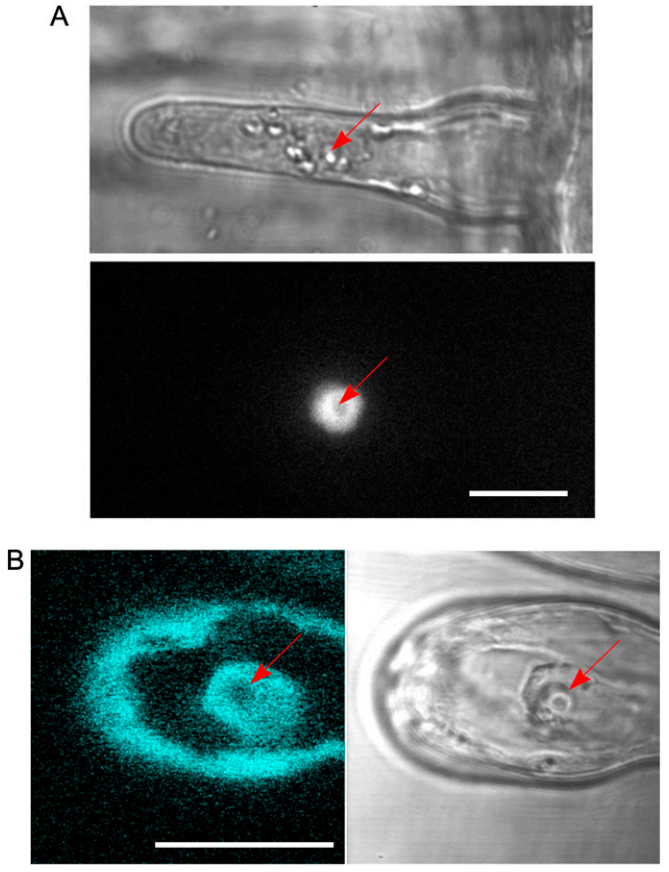

Fig. S1. YC2.1 localizes to the cytoplasm and the nucleoplasm of *M. truncatula* root hairs. (*A*) *Upper*: Transmission micrograph of a root hair expressing the nuclear targeted YC2.1 construct. The nucleus is indicated with an arrow. *Lower*: CFP fluorescence micrograph using confocal microscopy of the same root hair, indicating clear localization of yellow cameleon in the nucleus but not the nucleolus (dark spot inside the nucleus). This is consistent with what was previously reported (1). (*B*) Root hair expressing YC2.1 lacking the nuclear localization signal. *Left*: Confocal image showing CFP fluorescence of yellow cameleon YC2.1 in the cytoplasm and nucleus of the root hair. *Right*: Transmission light micrograph of the root hair in *A*. Red arrow indicates the nucleolus of the root hair cell. (Scale bar, 20 μm.)

1. Sieberer BJ, et al. (2009) A nuclear-targeted cameleon demonstrates intranuclear Ca^{2+} spiking in *Medicago truncatula* root hairs in response to rhizobial nodulation factors. *Plant Physiol* 151:1197–1206.

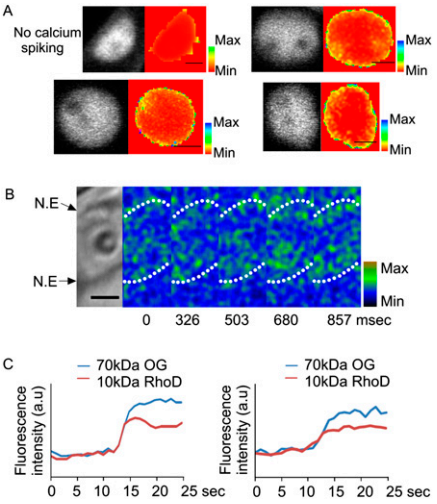

Fig. S2. Nuclear and cytoplasmic Nod factor-induced calcium transients in *M. truncatula* root hairs. (*A*) Maximum intensity stacks of four nuclei, three treated with Nod factor and one untreated, of plants expressing the nuclear-localized YC2.1. Each stack represents a single calcium transient, or an equivalent time period for the untreated cell. Note that the maximum calcium changes are associated with domains around the nuclear periphery. (Scale bars, 10 μm.) (*B*) Confocal images of a cell expressing YC2.1 lacking a nuclear localization signal. The left bright-field image indicates the presence of the nuclear envelope (N.E.), and the approximate location of the nuclear envelope is indicated with the dotted line. Images show a single calcium transient from its inception to its peak, with images 326 ms apart. Note that calcium changes (green) occur either side of the nuclear envelope. (Scale bar, 5 μm.) (*C*) Single calcium transients from two root hair cells of *M. truncatula* microinjected with Oregon Green fused to 70-kDa dextran (excluded from the nucleus) and RhoD fused to 10-kDa dextran (diffusible into the nucleus). Note that calcium changes measured using RhoD occur with a similar timing as those measured with Oregon Green.

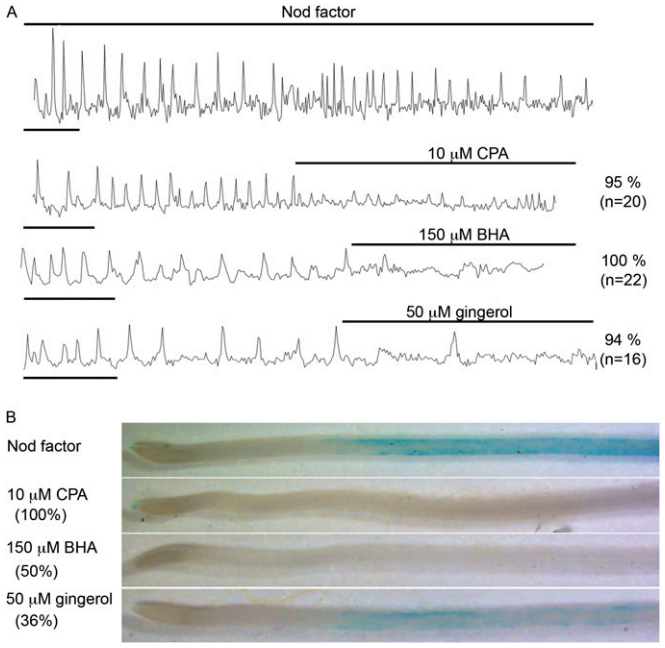

Fig. S3. Pharmacological evidence for the involvement of SERCA-type calcium ATPases in Nod factor-induced calcium spiking. (*A*) The SERCA-ATPase inhibitor cyclopiazonic acid (CPA) and the ATPase activators gingerol and butylated hydroxyanisole (BHA) suppressed Nod factor-induced calcium spiking. Percentage of cells showing calcium spiking inhibition is indicated. Number of cells tested is shown in brackets. The reductions in responding cells for all treatments is highly significant according to *t* tests, with *P* values <0.0001. The time bar at the bottom left of each trace represents 5 min. (*B*) These inhibitors also blocked Nod factor-induced gene expression as assayed with the Nod factor-specific reporter line *pENOD11*::GUS. Indicated in brackets is the percentage of roots in which the inhibition of *ENOD11-GUS* was observed. CPA inhibition of calcium spiking and *ENOD11* has been previously reported (1, 2).

1. Engstrom EM, Ehrhardt DW, Mitra RM, Long SR (2002) Pharmacological analysis of nod factor-induced calcium spiking in *Medicago truncatula*. Evidence for the requirement of type IIA calcium pumps and phosphoinositide signaling. *Plant Physiol* 128:1390–1401.
2. Charron D, Pingret JL, Chabaud M, Journet EP, Barker DG (2004) Pharmacological evidence that multiple phospholipid signaling pathways link Rhizobium nodulation factor perception in *Medicago truncatula* root hairs to intracellular responses, including Ca^{2+} spiking and specific ENOD gene expression. *Plant Physiol* 136:3582–3593.

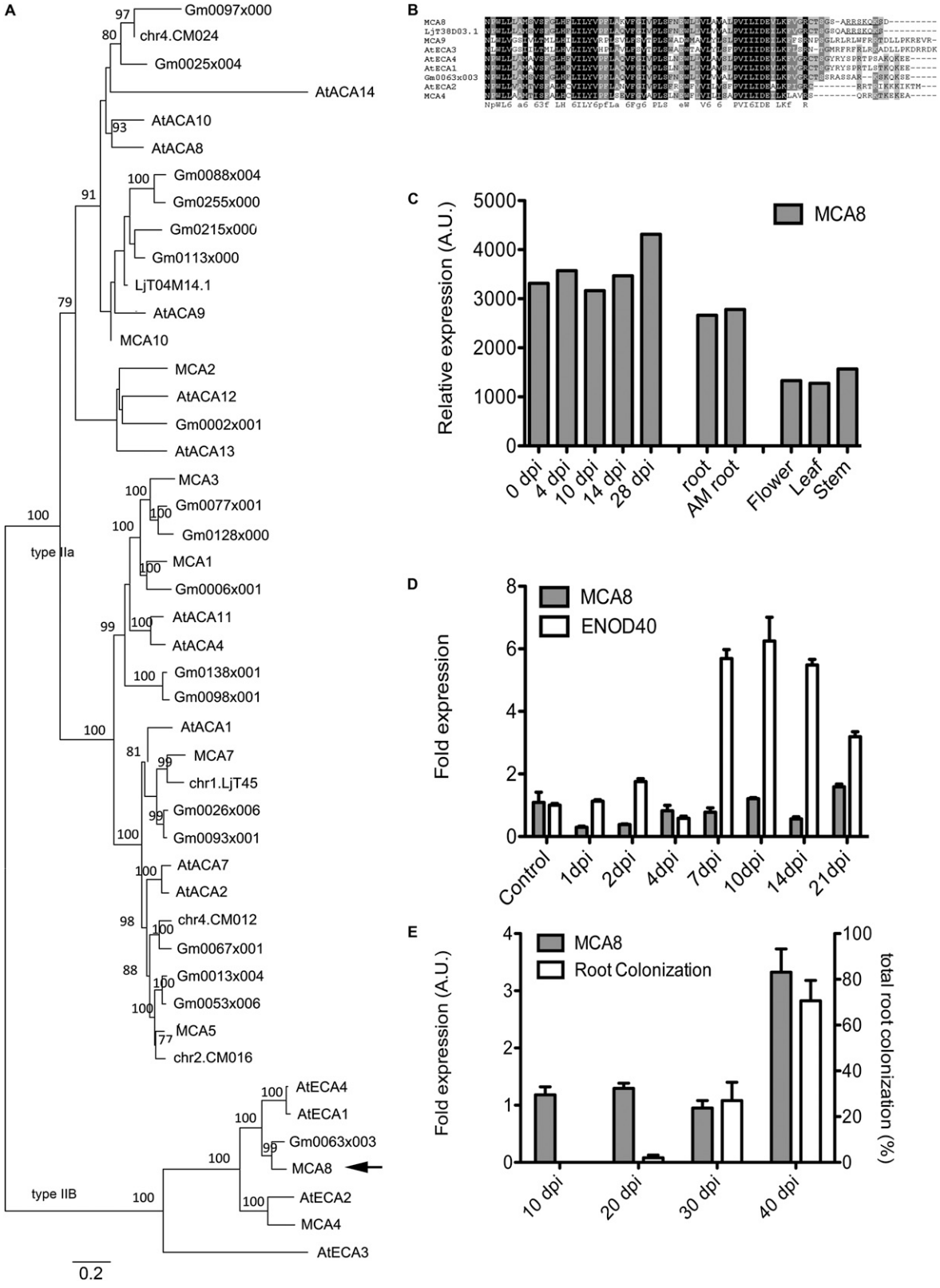

Fig. S4. Phylogenetic and expression analysis of *M. truncatula* ATPase genes. (*A*) Phylogenetic tree of the *M. truncatula* calcium ATPase gene family and comparison with soybean, *Lotus japonicus*, and *Arabidopsis* sequences. P-type ATPases are well conserved throughout plants, and subtypes IIA and IIB can be discerned easily on the basis of their sequences. (*B*) Alignment of the C terminus of the *M. truncatula* MCA8 protein sequence with similar sequences from *Arabidopsis*, *Lotus*, and soybean. The conserved nuclear localization signal is underlined in the *L. japonicus* and *M. truncatula* sequences. (*C–E*) Quantitative RT-PCR analysis of *MCA8*. (*C*) *MCA8* is not regulated during nodulation or mycorrhization in the *Medicago* gene atlas. (*D*) Expression of *MCA8* at different stages of nodulation. No induction is observed. *MtENOD40* is shown as a positive control. (*E*) During a mycorrhization time series, *MCA8* seems to be up-regulated at later stages of the interaction, when maximal arbuscule formation occurs. Also shown is the arbuscular mycorrhizal (AM) colonization percentages of samples used in the quantitative RT-PCRs. A.U., arbitrary units.

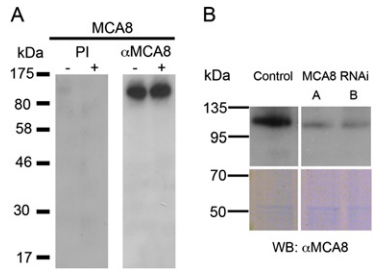

Fig. S5. Native MCA8 antibodies. (*A*) Western blot using polyclonal antibodies raised against MCA8 and the respective preimmune control (preimmune, PI). *M. truncatula* root samples (–) are compared with nodulated roots (+). The MCA8 antibody recognizes just one protein of the correct size. (*B*) Specificity control for the polyclonal antibodies. Control roots are compared with *MCA8* RNAi roots. Two pools, A and B, were generated of 10 roots containing the *MCA8* silencing construct. The MCA8 antibody shows a much-reduced signal in the roots where *MCA8* is silenced. The loading control is shown below. WB, Western blot; αMCA8, MCA8 antiserum.

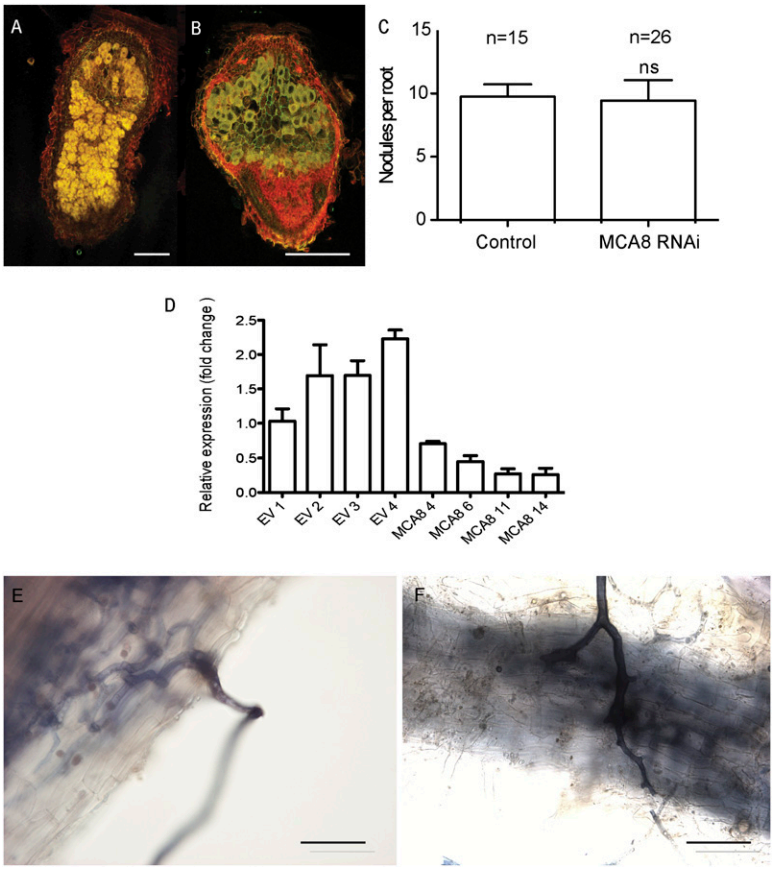

Fig. S6. Symbiosis phenotype of *MCA8* silenced roots. (*A–C*) Nodulation phenotype of *MCA8* RNAi roots. (*A*) Cross-section through a 21-d-old nodule on a control root; plant tissue is red owing to DsRED marker expression, and GFP-expressing rhizobia are yellow. (*B*) A nodule (21 d after inoculation) on an *MCA8* RNAi root. (*C*) Average nodule numbers per construct used, error bars are SEM. n = number of transgenic roots analyzed. Control = empty vector transformed. (*D*) Confirmation of the visual colonization measurements using quantitative RT-PCR on an arbuscule-specific plant gene *MtPT4* at 6 wk after inoculation. The numbers on the *x* axis indicate the name of the RNAi root used, and the percentages of expression levels are measured relative to the housekeeping gene in the control roots. Only four representative roots are shown per construct. EV, empty vector. (*E* and *F*) Wild-type (*E*) roots are easily colonized by penetration hyphae, whereas in *MCA8* silenced roots (*F*) multiple aborted attempts can be seen, accompanied by septate hyphae and swollen hyphopodia. (Scale bars, 1 mm in *A*, 0.1 mm in *B*, 100 mm in *E* and *F*.)

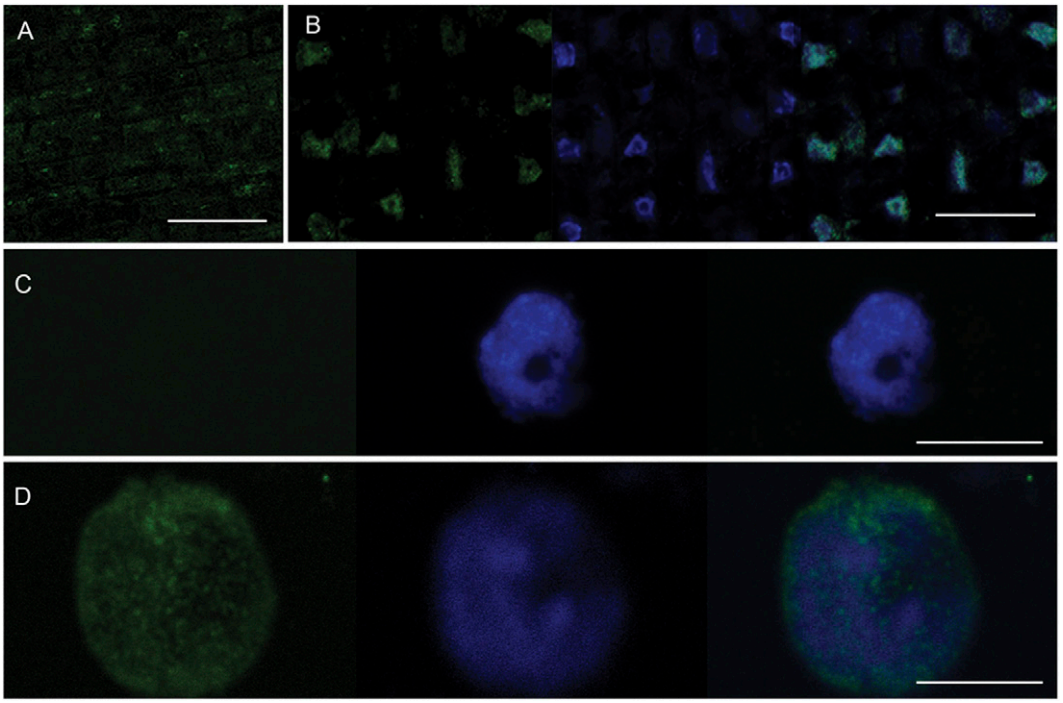

Fig. S7. Nuclear localization of MCA8. (*A–D*) Immunofluorescence using a polyclonal antiserum against MCA8 in fixed *M. truncatula* root tissue. (*A*) Preimmune serum control of MCA8: no significant signal is observed. (*B*) Immunofluorescent signal using an MCA8 antibody. *Left*: MCA8 immunolocalization (green); *Center*: DAPI staining for nuclear DNA; *Right*: merge. (*C*) Preimmune control for MCA8 on isolated nuclei of *M. truncatula* root cells. *Left*: Immunofluorescent signal; *Center*: DAPI staining for nuclear DNA; *Right*: merge. (*D*) As in *C*, but using a polyclonal antibody raised against MCA8. (Scale bars, 100 μm in *A*, 50 μm in *B*, 10 μm in *C* and *D*.)

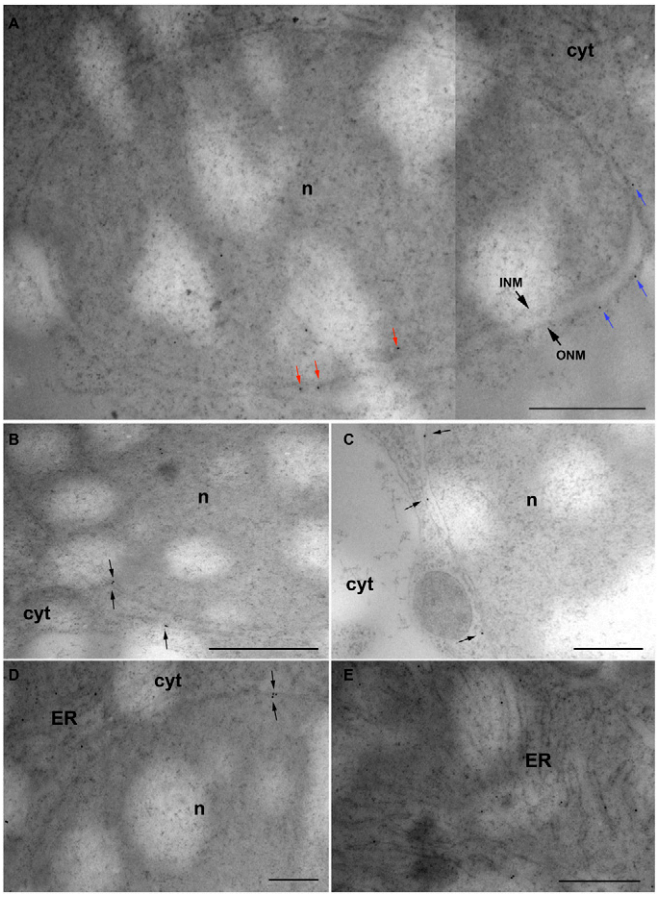

Fig. S8. Subcellular localization of MCA8 in root epidermal cells of *M. truncatula* quantified through immunogold labeling. (*A*) Merged image of a complete nucleus showing the localization of MCA8 on both inner (INM) and outer (ONM) nuclear membranes and on the endoplasmic reticulum (ER) membranes. (*B–D*) Localization of MCA8 on the inner and outer nuclear membranes on different nuclei sections, as observed by immunogold labeling. (*E*) Localization of MCA8 on the ER network as observed by immunogold labeling. Red arrow indicates gold particles on the inner nuclear membrane; blue arrow indicates gold particles on the outer nuclear membrane. n, nucleus; cyt, cytoplasm. (Scale bars, 500 nm.)